Disturbance-Rejection-Based Model Predictive Control: Flexible-Mode Design With a Modulator for Three-Phase Inverters

Hoach The Nguyen and Jin-Woo Jung, *Member, IEEE*

***Abstract*—This paper aims to investigate a disturbance-rejection-based model predictive control (MPC) with two flexible modes (i.e., unconstrained mode and constrained mode) for three-phase inverters with an LC filter. A disturbance observer (DOB) is designed to both simplify the prediction model and achieve the robustness against uncertain parameters. First, the unconstrained mode is designed with a simple horizon-one MPC control law to precisely regulate the output voltage in the steady state. Next, the constrained mode is designed with long-horizon MPC to quickly drive the system to the unconstrained mode by further optimizing the modulation stage. Also, the proposed MPC ensures the robustness and optimality in all operating modes. Especially, the overall closed-loop stability with DOB dynamics is proven by using Lyapunov function. Unlike other MPC methods, the long-horizon MPC in the constrained mode is specialized by finite switching sequences of the sector-based space vector modulation. Comparative studies with the conventional linear quadratic regulator are conducted on a prototype test bed with a TI TMS320F28335 DSP. Then, the proposed MPC method verifies fast dynamic response and advanced voltage regulation (i.e., small steady-state errors and low total harmonic distortion) under various load conditions and uncertain parameters.**

***Index Terms*—Model predictive control (MPC), optimal control, pulse-width modulation (PWM), space vector modulation (SVM), three-phase inverter.**

I. Introduction

THREE-PHASE voltage source inverters (3ϕ VSIs) with LC filters play a main role in power conversion systems such as distributed generation systems, energy storage systems, and uninterruptible power supplies [1]. The 3ϕ VSIs aim at supplying high-quality sinusoidal voltage with fast transient response, small steady-state error (SSE), and low total harmonic distortion (THD) under various load conditions such as load step change, unbalance load, and nonlinear load with diode rectifiers [2], [3].

Until recently, various control methods have been proposed to achieve the high-performance 3ϕ VSI such as proportional–integral (PI) based control [4]–[6], optimal control [7], adaptive control [8], [9], repetitive control [10]–[12], sliding mode control [13], [14], deadbeat control [15], [16], model predictive control (MPC) [17]–[26], etc. First, PI-based control [4]–[6] is simple, but it needs careful gain tuning, which is hard to optimize the closed-loop performances. In addition, the stability is not guaranteed in case of input constraints violated or uncertain model. Optimal control [7] can optimize the closed-loop performance with an explicit index but the optimal problem becomes tough with constraints and nonlinearity. Hence, the control methods in [4]–[7] face the difficulty on input constraints in which the control law is fragile by the control input saturation. Adaptive control [8], [9] and repetitive control [10]–[12] are effective in the system changes such as fluctuating loads, parameter variations, etc. However, these two methods are complicated in computation and gains selection. Sliding mode control [13], [14] can deal with bounded parameter variations. However, the switching structure brings a chattering problem that can degrade the output quality. Next, deadbeat control [15], [16] offers good dynamic responses, however its aggressive performance is sensitive to disturbances or parameter mismatches, and it is usually fragile due to the input constraints.

Recently, MPC has been applied into the power electronics area by two approaches: continuous control set (CCS) [17], [18] and finite control set (FCS) [19]–[25]. When the control inputs are considered as bounded continuous variables in the CCS approach, explicit MPC can offers an offline solution implemented by a modulator. However, the inclusion of the constraints or model nonlinearity makes the optimization complicated and there is no explicit solution for the CCS-MPC with complex constraints or nonlinear models [26]. Consequently, this approach exhibits good performances around the desired steady state and proves asymptotic stability [18], [25] in case that the linearized model around the steady state is used. Second, the FCS-MPC takes the advantages of the finite switching vectors or finite switching sequences of the power converters to solve the optimization problem [27]. Due to the limited options (i.e., discrete switching vectors or switching sequences) in

Manuscript received February 14, 2017; revised June 7, 2017, July 10, 2017, and August 21, 2017; accepted September 14, 2017. Date of publication October 2, 2017; date of current version January 5, 2018. This work was supported by the National Research Foundation of Korea under Grant 2015R1A2A2A01003513 funded by the Korea government (Ministry of Science, ICT, and Future Planning). *(Corresponding author: Jin-Woo Jung.)*

The authors are with the Division of Electronics and Electrical Engineering, Dongguk University, Seoul 04620, Korea (e-mail: jinwjung@dongguk.edu).

Color versions of one or more of the figures in this paper are available online at http://ieeexplore.ieee.org.

Digital Object Identifier 10.1109/TIE.2017.2758723

a short prediction horizon, the FCS-MPC can be implemented online without computational burden. Recently, the FCS-MPC becomes well-known in power electronics as a direct method where a modulator is not necessary [23]–[26] in an optimal switching vector (OSV) MPC or a modulator is imitated in an optimal switching sequence (OSS) MPC [27]. Also, the distinct properties of the FCS-MPC are the fast dynamic response flexible objectives and constraints inclusion [21]–[23]. However, the conventional OSV-FCS approach results in variable switching frequency, high sampling frequency, and high-ripple outputs [21]. The stability analysis is also a challenging issue to the FCS-MPC [26], and the ultimate bounded region is proven to strengthen this approach [24]–[26]. Commonly, the FCS methods have been reported with high SSEs [21], [22].

A switched MPC strategy [25] combines the advantages of both approaches (i.e., CCS-MPC and FCS-MPC) with two separated control laws. That is, the FCS-MPC with a nonlinear model can direct the system states toward a bounded region of the desired equilibrium state, and then the control law is switched into a linear CCS-MPC to asymptotically reach the reference. However, the switched control strategy of the MPC uses two separated control laws with duplicated computational effort, and the robustness of the MPC-based approach due to the model mismatches and noises is still questionable. In [25], a solution based on a hysteresis band is presented to avoid false triggering due to the noises. However, online computation for switching criteria such as the hysteresis band occupies more allowable time of the overall algorithm. Finally, there are still open issues for the MPC methodology such as: the online computational efficiency; the robustness against model mismatches and noises; and the usage of a modulation stage.

This paper proposes a disturbance-rejection-based MPC with two flexible modes (i.e., unconstrained mode and constrained mode) for three-phase VSIs with an LC filter. The discrete-time disturbance observer (DOB) is designed under disturbance-rejection approach to at once compensate for the model uncertainties and simplify the prediction model. A simple horizon-one (H-1) MPC control law is developed for the unconstrained mode whenever the constraints are satisfied to accurately regulate the output voltages in the steady state. Interestingly, the H1-MPC law in the unconstrained mode can turn into two control laws designed by linear quadratic regulator (LQR) and deadbeat controller. Also, the constrained mode is designed to quickly drive the system to the unconstrained mode with long-horizon MPC. The constrained mode is dedicated to the transient performance that uses the long-horizon prediction to deal with the fast dynamics. In particular, the overall closed-loop system stability with DOB dynamics is proven based on a Lyapunov function. Unlike other MPC methods, the long-horizon MPC in the constrained mode further optimizes the modulation stage by utilizing the finite switching sequences of a space vector modulation (SVM) technique. Comparative studies with the conventional LQR are carried out on an experimental test bed with a TI TMS320F28335 DSP. Finally, the comparative results demonstrate that the proposed MPC method guarantees the faster dynamic responses and better steady-states regulation (e.g., smaller SSE and lower THD) compared to the conventional LQR under various load disturbances and model mismatches.

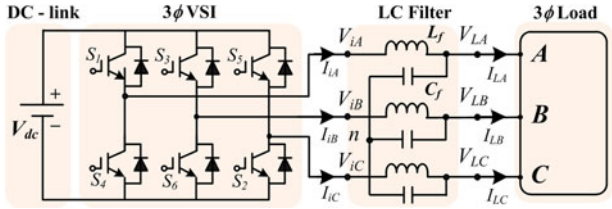

Fig. 1. Three-phase VSI with an LC filter.

II. State-Space Model for Direct Voltage Prediction

This section derives the discrete-time state-space model of a typical three-phase inverter with an LC filter to use a disturbance-rejection control approach. As shown in Fig. 1, the electric quantities are defined as the inverter line-to-neutral voltage vector $\bar{\boldsymbol{V}}_i = [V_{iA}\ V_{iB}\ V_{iC}]^T$, the inverter phase current vector $\bar{\boldsymbol{I}}_i = [I_{iA}\ I_{iB}\ I_{iC}]^T$, the load line-to-neutral voltage vector $\bar{\boldsymbol{V}}_L = [V_{LA}\ V_{LB}\ V_{LC}]^T$, and the load phase current vector $\bar{\boldsymbol{I}}_L = [I_{LA}\ I_{LB}\ I_{LC}]^T$, respectively.

The mathematic model of the LC filter is developed in the synchronously rotating $d-q$ reference frame by using *Kirchoff's laws* and discretized by using a forward Euler method as follows [8], [18]:

$$\begin{cases} V_L(k+1) = AV_L(k) + k_C t_s \left[I_i(k) - I_L(k)\right] \\ I_i(k+1) = AI_i(k) - k_L t_s \left[V_L(k) - V_i(k)\right] \end{cases} \tag{1}$$

where $A = \begin{bmatrix} 1 & \omega t_s \\ -\omega t_s & 1 \end{bmatrix}$, $k_C = 1/C_f$, $k_L = 1/L_f$, ω is the electric angular frequency, t_s is the sampling time, $V_i(k) = [V_{id}(k),\ V_{iq}(k)]^T$ is the inverter voltage vector (i.e., control input), $V_L(k) = [V_{Ld}(k),\ V_{Lq}(k)]^T$ is the load voltage vector (i.e., controlled output), $I_i(k) = [I_{id}(k),\ I_{iq}(k)]^T$ is the inverter current vector (i.e., state variables), and $I_L(k) = [I_{Ld}(k),\ I_{Lq}(k)]^T$ is the load current vector (i.e., unknown disturbance). Note that k represents the kth sampling instant of the discrete-time quantities. However, the symbol k is omitted for a short expression in the following parts because all the equations are interpreted in the discrete-time domain. Similarly, to represent the $(k+1)$ and $(k+2)$ instants, this paper uses the superscript $(+)$ and $(++)$, respectively. Also, the reference load voltage vector in the $d-q$ frame denoted as $V_L^* = [V_{Ld}^*,\ V_{Lq}^*]^T$ is a constant vector.

Conventionally, the MPC methods for 3ϕ VSIs can utilize the model (1) to predict the system states [18]–[20]. However, in order to prove the stability using a Lyapunov function and take the advantages of the simple error-model-based prediction, the error dynamic model is needed to be derived as follows. First, the equilibrium state of the system (1) is identified as $X^* = [V_L^{*\,T},\ I_i^{*\,T}]^T = [V_{Ld}^*,\ V_{Lq}^*,\ I_{id}^*,\ I_{iq}^*]^T$ where the state variables of the model (1) are unchanged. Hence, the inverter current $I_i^* = [I_{id}^*,\ I_{iq}^*]^T$ and control input $V_i^* = [V_{id}^*,\ V_{iq}^*]^T$ in the equilibrium state are inferred from (1) as

$$I_i^* = I_L - C_f A_0 V_L^*,\ V_i^* = V_L^* - L_f A_0 I_i^* \tag{2}$$

where $A_0 = \begin{bmatrix} 0 & \omega \\ -\omega & 0 \end{bmatrix}$.

Then, the following error vectors are introduced to develop the error dynamic model:

$$V_{Le} = V_L - V_L^*,\ I_{ie} = I_i - I_i^*,\ V_{ie} = V_i - V_i^*. \quad (3)$$

Finally, the error dynamic model of the LC filter is achieved by substituting (3) into (1) as follows:

$$V_{Le}^+ = AV_{Le} + k_C t_s I_{ie} \quad (4)$$

$$I_{ie}^+ = AI_{ie} - k_L t_s V_{Le} + k_L t_s V_{ie}. \quad (5)$$

Equations (4) and (5) represent a second-order system with one input vector $V_{ie} \in R^{2\times 1}$ and one output vector $V_{Le} \in R^{2\times 1}$. For simplicity, a matrix-based representation is adopted as

$$X_e^+ = \Phi X_e + \Gamma V_{ie} \quad (6)$$

where $\Phi = \begin{bmatrix} A & k_C t_s I_{2\times 2} \\ -k_L t_s I_{2\times 2} & A \end{bmatrix}$, $\Gamma = \begin{bmatrix} O_{2\times 2} \\ k_L t_s I_{2\times 2} \end{bmatrix}$, $X_e = [V_{Le}^T, I_{ie}^T]^T$, and $I_{m\times n}$ and $O_{m\times n}$ are the identity matrices and zero matrices with the relevant sizes (m rows, n columns), respectively.

By substituting (5) into (4), two-step ahead direct voltage prediction, $V_{Le}(k+2)$ with respect to the state $X_e(k)$ and control input $V_{ie}(k)$ can be derived as follows:

$$V_{Le}^{++} = \Lambda X_e + \Pi V_{ie} \quad (7)$$

where $\Lambda = [A^2 - k_C k_L t_s^2 I_{2\times 2}\ 2k_C t_s A]$ and $\Pi = k_C k_L t_s^2 \in R$.

The one-step deadbeat control law [26] can be easily set up by letting $V_{Le}^{++} = 0$ in (6)

$$V_{ie} = -\Pi^{-1}\Lambda X_e. \quad (8)$$

III. Disturbance-Rejection-Based H-1 MPC Design

This section derives the DOB based H-1 MPC in which the lumped quantities of possible disturbances are simultaneously estimated. Then, these estimates compensate for both the model prediction and the control input to achieve the robustness against the disturbances.

A. Discrete-Time DOB Design

The state variables (V_L^*, I_i^*) and control input (V_{id}^*, V_{iq}^*) in the equilibrium state can be identified from (2) using the load current sensors and nominal LC parameters. However, using the external sensors to measure the load currents could increase the system cost and vulnerability. Furthermore, the model-based calculation using (2) directly depends on the LC values, which are uncertain. Therefore, these terms should be estimated from the input control V_i and the available measured variables $(V_L,\ I_i)$ to achieve the robust MPC via the disturbance-rejection approach.

The significant benefit of the total disturbance estimation approach is that the model can be simplified with a certain understanding of the system dynamics. Other mismatches can be estimated as the lump quantities. It is worth noting that the voltage reference V_L^* is known and the load current I_L varies slowly in comparison with the dynamics of state variables during a small sampling period [7], [9], [20] in the $d-q$ frame. Furthermore, due to the slow variations of the LC values in operation, the equilibrium variables in (2) are assumed to change slowly (i.e., $I_i^{*+} = I_i^*$, $V_i^{*+} = V_i^*$) during a small sampling period [8], [20]. Then, the augmented dynamic model for the DOB can be derived by combining the error dynamic model (4), (5) and the steady-state dynamics ($I_i^{*+} = I_i^*$, $V_i^{*+} = V_i^*$), which is rewritten in the matrix form as

$$X_0^+ = A_0 X_0 + B_0 V_i,\ Y_0 = C_0 X_0 \quad (9)$$

where

$$X_0 = \left[V_{Le}^T, I_i^T, I_i^{*T}, V_i^{*T}\right]^T,\ Y_0 = \left[V_{Le}^T, I_i^T\right]^T,$$

$$C_0 = [I_{4\times 4}, O_{4\times 4}]$$

$$A_0 = \begin{bmatrix} A & k_C t_s I_{2\times 2} & -k_C t_s I_{2\times 2} & O_{2\times 2} \\ -k_L t_s I_{2\times 2} & A & -A & -k_L t_s I_{2\times 2} \\ O_{2\times 2} & O_{2\times 2} & I_{2\times 2} & O_{2\times 2} \\ O_{2\times 2} & O_{2\times 2} & O_{2\times 2} & I_{2\times 2} \end{bmatrix}$$

$$B_0 = [O_{2\times 2}, k_L t_s I_{2\times 2}, O_{4\times 2}]^T.$$

Next, the DOB is represented by the following equations [28]:

$$\begin{cases} \hat{X}_0^+ = A_0 \hat{X}_0 + B_0 V_i + L_0 C_0 [X_0 - \hat{X}_0] \\ \hat{X}_d = \left[\hat{I}_{id}^*, \hat{I}_{iq}^*, \hat{V}_{id}^*, \hat{V}_{iq}^*\right]^T \end{cases} \quad (10)$$

where $\hat{X}_0$ is an estimate of X_0 and $L_0 \in R^{8\times 4}$ is the observer gain matrix.

Then, the error dynamics of the DOB is obtained by subtracting (10) from (9) given by

$$X_{0e}^+ = (A_0 - L_0 C_0) X_{0e} = A_{0LC} X_{0e} \quad (11)$$

where $X_{0e} = X_0 - \hat{X}_0$ and $A_{0LC} = A_0 - L_0 C_0$.

The gain matrix L_0 is optimized by the following calculation:

$$L_0 = A_0 K_0 C_0^T \left(R_0 + C_0 K_0 C_0^T\right)^{-1} \quad (12)$$

where $K_0 \in R^{8\times 8}$ is the solution of the discrete-time algebraic Riccati equation (DARE) [28]:

$$A_0 \left[K_0 - K_0 C_0^T \left(R_0 + C_0 K_0 C_0^T\right)^{-1} C_0 K_0\right] \Phi_0^T - K_0 + Q_0 = 0 \quad (13)$$

where $Q_0 \in R^{8\times 8}$ is a symmetric positive-semidefinite matrix and $R_0 \in R^{4\times 4}$ is a symmetric positive-definite matrix, which denote the covariance matrices representing the Gaussian white noise considered as the design parameters. Note that these design parameters are simplified as $Q_0 = \lambda R_0$, where λ is a positive real number representing the ratio between Q_0 and R_0 (i.e., between the measurements and the process noise).

Let the Lyapunov function be selected as the following:

$$V_0 = X_{0e}^T K_0 X_{0e}$$

$$\Delta V_0 = V_0^+ - V_0 = X_{0e}^T \left(-Q_0 - L_0 R_0 L_0^T\right) X_{0e} \le 0. \quad (14)$$

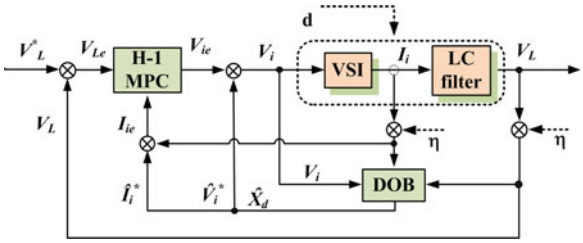

Fig. 2. Block diagram of the disturbance-rejection-based H1-MPC for a three-phase VSI with an LC filter.

This implies that A_{0LC} is a stable matrix and X_{0e} is exponentially stable.

Remark 1: Fig. 2 illustrates the block diagram of the disturbance-rejection H1-MPC for a three-phase VSI with an LC filter where d and η are the process and measurement disturbances/noises, respectively. As depicted in Fig. 2, after compensating for the model (via I_i^*) and input control (via V_i^*), the model-based control (e.g., MPC) is proposed with two control modes. That is, as soon as the DOB can observe the disturbances, the controller can reject these disturbances to achieve the robustness regardless of the operating modes. Thus, the DOB can both estimate the disturbances and deal with the noises as

$$I_i^* = I_L - C_f A_0 V_L^* + d_i,\ V_i^* = V_L^* - L_f A_0 I_i^* + d_v \quad (15)$$

where C_f and L_f denote the available values of capacitance and inductance of an LC filter, and d_i and d_v represent other process disturbances. The steady-state Kalman–Bucy filter observer gains given by (12) and (13) rely on the statistical conditional probability of the noises presented by two covariance matrices (Q_0 and R_0) [18], [20]. The DOB-based prediction can improve the noise immunity of the proposed MPC scheme with suitable values of the covariance matrices that will be practically investigated in Section V-C. The key point for the robustness in all operating modes is that the compensated model is utilized for both modes. Consequently, the robustness can be achieved by the following control design.

B. DOB-Based H1-MPC Design

The H-1 MPC is derived from the optimization problem with the following quadratic objective function:

$$J(V_{ie}) = \left\|V_{Le}^{++}\right\|_P^2 + \|V_{ie}\|_R^2 \quad (16)$$

where P, $R \in R^{2\times 2}$ are positive-definite weighting matrices, and $\|.\|_P^2 = (.)^T P(.)$ is a quadratic form. Note that the objective function (16) is based on the estimation of total disturbance $\hat{X}_d = [\hat{I}_i^{*T}, \hat{V}_i^{*T}]^T$ as shown in Fig. 2, where both the prediction and the control input are compensated for to reject the disturbance.

By directly substituting (7) into (16), the objective function is rewritten as

$$J = X_e^T \Lambda^T P \Lambda X_e + 2X_e^T \Lambda^T P \Pi V_{ie} + V_{ie}^T (\Pi^T P \Pi + R) V_{ie}. \quad (17)$$

Taking the partial derivative of (17) with respect to V_{ie}, the global optimal solution of this quadratic function is achieved as

$$\frac{\partial J}{\partial V_{ie}} = 0 \Leftrightarrow V_{ie}^{uc} = -(\Pi^T P \Pi + R)^{-1} \Pi^T P \Lambda X_e. \quad (18)$$

The solution (18) shows a familiar linear feedback optimal control law with the optimal gain [29] given by:

$$K = -(\Pi^T P \Pi + R)^{-1} \Pi^T P \Lambda. \quad (19)$$

From this solution, the disturbance-rejection-based optimal control law can be expressed by

$$V_i^{uc} = K(X - \hat{X}^*) + \hat{V}_i^*. \quad (20)$$

Specially, the above-mentioned result (20) is obtained from an H-1 MPC approach without solving any Ricatti-like equation. If the weighting matrix P is chosen as the solution of the following DARE [28]:

$$\Lambda^T \left[P - P\Pi(\Pi^T P \Pi + R)^{-1} \Pi^T P\right] \Lambda - X + Q = 0 \quad (21)$$

where $P = C^T X C$ and $C = [I_{2\times 2}, O_{2\times 2}]^T$, then, the above-mentioned control law turns into the well-known steady-state LQR that minimizes the following cost function [29]:

$$J = \sum_{i=0}^{\infty} \left[X_{Le}^T(k) Q X_{Le}(k) + V_{ie}^T R V_{ie}\right]. \quad (22)$$

Due to this simple approach, the proposed method can achieve the flexibility of the objective function by properly adjusting P and R in design.

Remark 2: The control law (18) is an unconstrained solution of the H1-MPC if the constrained input is not violated [18], [26]. This kind of control law has been successfully applied in [7], [18], and [25] in the steady state with an SVM technique without considering the constraints of manipulated variables [18]. Section IV will take into account these constraints by two different modes (i.e., unconstrained mode and constrained mode).

IV. Disturbance-Rejection-Based Flexible-Mode MPC Design With a Modulation Stage

This section proposes an MPC method with two flexible modes (i.e., unconstrained mode and constrained mode). First, an H1-MPC law is designed with a standard SVM technique for the unconstrained mode if (20) does not violate the input constraints [18], [26]. Second, a special SVM-based long-horizon MPC law with optimal switching instants is proposed for the constrained mode if (20) is not feasible because of the input constraints. In this paper, the proposed MPC offers the flexibility because different performance indexes can be chosen independently for each mode. Furthermore, the online change of performance index is allowed by the online solution in the constrained mode, which is selected from finite switching sequences in a fashion like FCS-MPC.

A. H-1 MPC Design for Unconstrained Mode

The unconstrained mode is defined as the mode where the H-1 MPC control law (20) does not violate the input constraints

determined by the SVM limitations [18], [26] as

$$\sqrt{3}\,|V_{i\alpha}(k+1)| + |V_{i\beta}(k+1)| \le \frac{2}{\sqrt{3}}V_{dc},\ |V_{i\beta}(k+1)| \le \frac{V_{dc}}{\sqrt{3}} \tag{23}$$

where $V_{i\alpha}$ and $V_{i\beta}$ are the control input in the stationary $\alpha-\beta$ reference frame. The constraint (23) is the limitation of the SVM represented by a hexagonal boundary. However, in practice, this constraint is simplified by the inner circle of the hexagon due to the unavoidable switching delay and limited switching frequency of the power switches [18]. It is noted that the unconstrained mode is dedicated to precisely regulating the output voltages in the steady state where the optimal control input (20) is directly applied through the standard SVM stage.

In this section, the overall stability of the H-1 MPC (i.e., optimal control) law (20) is proven using Lyapunov stability theory. The asymptotic stability is guaranteed for the DOB-based optimal control where the dynamics of the DOB is taken into account. First, the control law (20) is rewritten with the estimated disturbances as follows [7]:

$$V_i = KX_e + V_i^* + HX_{0e} \tag{24}$$

where $H = [K, -I_{2\times2}]C_{6\times8}$, $C_{6\times8} = \begin{bmatrix} O_{2\times4} & O_{2\times4} \\ O_{4\times4} & I_{4\times4} \end{bmatrix}$.

Then, the Lyapunov function is selected as

$$V(X_e, X_{0e}) = V_{Le}^T P V_{Le} + \mu X_{0e}^T P_0 X_{0e} \tag{25}$$

$$\Delta V = V(k+1) - V(k) = -\begin{bmatrix} X_e^T, & X_{0e}^T \end{bmatrix} \Xi \begin{bmatrix} X_e^T \\ X_{0e}^T \end{bmatrix} \tag{26}$$

where μ is a scalar and

$$\Xi = \begin{bmatrix} Q + K^T RK & -(\Lambda + \Gamma K)^T P \Pi^T H \\ -H^T \Pi P(\Lambda + \Pi K) & \mu(Q_0 + L_0 R_0 L_0^T) - H^T \Pi^T P \Pi H \end{bmatrix}.$$

In (26), the condition for $\Delta V < 0$ (and $\Delta V = 0$ only at the desired equilibrium state) implies that the scalar μ is sufficiently large as the following:

$$\mu\left(Q_0 + L_0 R_0 L_0^T\right) > H^T \Pi^T P \Pi H + H^T \Pi P(\Lambda + \Pi K)(Q + K^T RK)^{-1}(\Lambda + \Gamma K)^T P \Pi^T H. \tag{27}$$

To this end, the proposed DOB-based H1-MPC system achieves the asymptotic stability. However, this stability is proven with the assumption on the feasibility of the optimal control input (20). In this paper, when the input constraint (23) is violated, the following constrained mode is proposed by utilizing the unconstrained solution (20) and the sector-based switching pattern of the SVM.

B. Long-Horizon MPC Design for Constrained Mode

This section elaborates the long-horizon MPC for the constrained mode in order to further optimize the modulation stage via an approach like FCS-MPC. It is noted that the constrained mode is dedicated to the transient performance that deals with the fast dynamics.

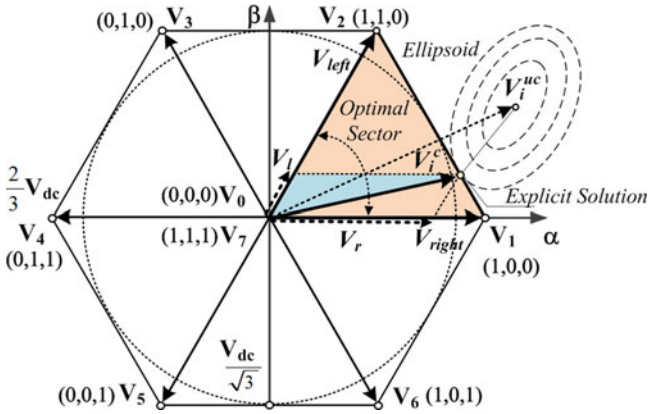

Fig. 3. Sector-based switching pattern of an SVM.

Fig. 3 illustrates the sector-based switching pattern of an SVM. As depicted in Fig. 3, it is assumed that the explicit optimal vector for the constrained case is known as V_i^C. Then, in the conventional SVM, V_i^C is represented by the vector addition of two adjacent basic vectors V_{right} and V_{left} as follows:

$$V_i^C = V_r + V_l \approx \frac{T_{\text{right}}}{T_z}V_{\text{right}} + \frac{T_{\text{left}}}{T_z}V_{\text{left}} \tag{28}$$

where $T_{\text{right}} = T_z\frac{|V_r|}{|V_{\max}|}$, $T_{\text{left}} = T_z\frac{|V_l|}{|V_{\max}|}$, $|V_{\max}| = \frac{2}{3}V_{dc}$, and T_z is one pulse-width modulation (PWM) period. It is worth noting that in this constrained mode, only active basic vectors are used to obtain the maximum reference vector (i.e., zero vectors V_0 and V_7 are not used). The approximation of V_i^C by the above-mentioned proportional time span (i.e., T_{left} and T_{right} within T_z) of the adjacent basic vectors in the conventional SVM does not consider the system dynamics within T_z (i.e., switching period in SVPWM). However, the dynamics in the transient state is often fast, so the long-horizon prediction within T_z is considered to optimize the modulation stage in the proposed long-horizon MPC as detailed below.

In Fig. 3, the switching sequences within T_z with respect to the sector-based switching pattern of the SVM in the optimal sector are represented by $\tilde{V}_i = [V_{i0}, V_{i1}, \ldots, V_{iN-1}] = [V_{\text{right}}, V_{\text{right}}, \ldots, V_{\text{left}}, V_{\text{left}}]$ where N is the prediction horizon, and V_{right} and V_{left} are two adjacent basic vectors. Each basic vector $(V_{\text{right}}, V_{\text{left}})$ in the switching sequence is held in a sampling time t_s. Therefore, $N = T_z/t_s$, and in each T_z, there are $(N+1)$ possible options for the switching sequence that depends on the switching instant from V_{right} to V_{left}.

Fig. 4 illustrates the finite switching sequences of the proposed SVM based long-horizon MPC with $N = 6$ for the constrained mode. In Fig. 4, there are seven options $(N^* = 0, 1, 2, \ldots, 6)$ of the control sequence with respect to the switching instant from V_{right} to V_{left}. Then, the final state X_{eN} from the initial system state (X_e) with respect to each control sequence, $\tilde{V}_{ie} = [V_{ie0}, V_{ie1}, \ldots, V_{ieN-1}]^T$, is recursively

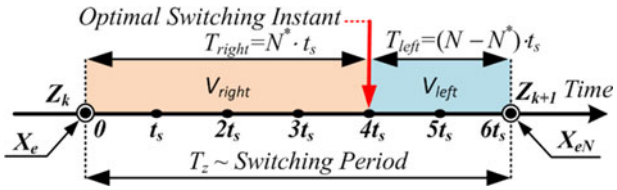

Fig. 4. Finite switching sequences of the proposed long-horizon MPC with $N = 6$ for the constrained mode.

predicted by using (6) as given by the following equation:

$$X_{eN} = \Psi \tilde{V}_{ie} + \Phi^N X_e \tag{29}$$

where $\Psi = [\Phi^{N-1}\Gamma,\ \Phi^{N-2}\Gamma,\ ...,\ \Phi\Gamma,\ \Gamma]$.

The MPC optimization problem is once again stated for horizon-N prediction as follows:

$$N^* = \text{Argmin}\left(\|X_{eN}\|_Q^2\right),\ N^* = \{0,\ 1,\ \ldots,\ N\}. \tag{30}$$

Now, the problem (30) is interpreted as finding the optimal switching instant N^* (i.e., switching from V_{right} to V_{left}) within $N + 1$ options (i.e., $0 - N$). To solve (30), a direct evaluation of all switching sequences is implemented in a fashion like the FCS-MPC that takes advantage of an online solution for the flexible-mode design [25].

In summary, the proposed long-horizon MPC inherits the advantages of the SVM such as a fixed switching frequency, low THD, etc., [26] by adopting the optimal-sector-based switching pattern. A long-horizon prediction (N) is further used in addition to the H1-MPC in this mode because the dynamics in the transient state is often fast. Unlike other modulation stages, the on-duty time of each adjacent active vector is optimized by considering the system dynamics via the model prediction based objective function (30). Furthermore, an online solution offers the flexibility of the objective function and constraints inclusion [23].

Remark 3: The model-based prediction (29) can be generalized with different nonlinear models and different discretion methods, which are not limited to the explicit forward Euler method. This paper employs the forward Euler method by considering its simple computation and acceptable accuracy in the context of a short horizon prediction (i.e., $N = 1$ in the unconstrained mode and $N \leq 6$ in the constrained mode) as widely used in literature [19], [22]–[25]. Unlike other MPC methods, this approach is a novel combination of the CCS-MPC and the OSS-MPC (i.e., one type of the FCS-MPC [27]) to both fix the switching frequency and simplify the OSS-MPC with an SVM.

V. Experimental Studies

This section validates the feasibility of the proposed flexible-mode MPC by experiments. First, the dynamic responses are investigated under a reference step-change condition to see the transient performances of the proposed long-horizon MPC method. Second, the robustness is evaluated under a load step-change condition with incorrectly set values of L, C parameters. Finally, the comparative studies with the LQR [7] under comprehensive scenarios are conducted to prove more advantageous

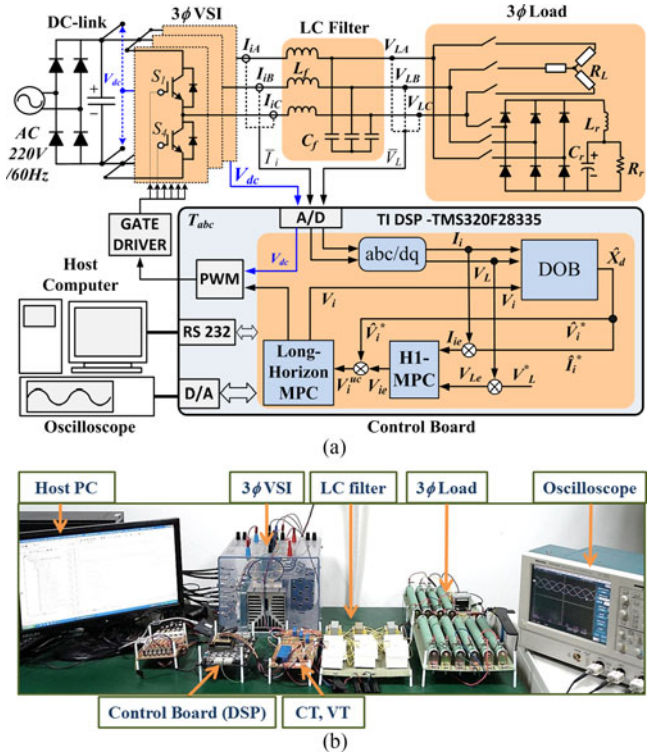

Fig. 5. Experimental setup of a prototype three-phase inverter test bed. (a) Overall schematic diagram. (b) Photograph of an experimental hardware.

performances of the proposed MPC scheme. Note that the conventional LQR is selected as a clear competitor of the proposed MPC method because the H-1 MPC law developed in Section III–B can turn into the LQR if the weighting matrix P is properly selected by the solution of the DARE (21). Besides, the LQR is a well-developed method with a clearly defined performance index. For a fair comparison, the objective function, sampling/switching frequency, testing scenarios, and LC parameters for the two control schemes are selected with the same values in the following studies. In this paper, the fundamental frequency based THD (THD_F) and the rms-based SSEs are used to evaluate the steady-state performances. Also, the THD_F is calculated from the spectrum analyzer of the oscilloscope in the range of 60 Hz−30 kHz, which includes the switching frequency and its significant harmonics. Next, the transient-state performances are evaluated via the dip voltage, the spike (overshoot) voltage, the settling time for the reference tracking performance, and the recovering time under sudden disturbances. It is noted that these performance criteria are extensively used in the literature [4], [7]–[13], [16].

A. Hardware Configuration

The overall hardware configuration for experiments is depicted in Fig. 5, where the three-phase inverter is controlled by a DSP via a gate driver. In the power circuit, a single-phase voltage source of ac 220 V_{rms}/60 Hz is rectified to supply a dc-link voltage of 295 V_{dc} to the inverter. As shown in Fig. 5(a), the dc-link voltage V_{dc} is fed back to the control algorithm to avoid

TABLE I
MAIN PARAMETERS OF THE EXPERIMENTAL SETUP

3ϕ VSI rated power	2000 VA
DC-link voltage (V_{dc})	295 V
Filter capacitance (C_f)	6.6 μF
Filter inductance (L_f)	10 mH
Switching/sampling frequency (f_{sw}/f_s)	5 kHz/20 kHz
Load rms reference voltages $(\mathbf{V}_{L,\mathrm{rms}})$	110 V
Fundamental frequency (f_1)	60 Hz

the deterioration in the load-voltage regulation against fluctuated V_{dc}. A 2-kVA-class three-phase inverter is connected to an LC filter (i.e., $L_f = 10$ mH, $C_f = 6.6$ μF) that is designed by considering a tradeoff between the system efficiency and the hardware cost. Fig. 5(a) and (b) exhibits the overall schematic diagram and photograph of our prototype experimental setup, respectively. In the test bed shown in Fig. 5(a), there are two types of loads: a Y-connected three-phase resistive load and a three-phase diode rectifier load. Also, the digital control system with a TI TMS320F28335 DSP receives the dc-link voltage (V_{dc}), the inverter currents $(\bar{I}_i)$, and load voltages $(\bar{V}_L)$ measured by the voltage and current transducers (VTs and CTs), and then it generates the control signals to the insulated-gate bipolar transistors (IGBTs) of the three-phase inverter via a gate driver.

In this paper, the control target is to provide the load with the sinusoidal voltage of 110 V_{rms}/60 Hz. It is noted that all control methods in this paper use the sampling frequency (f_s) of 20 kHz and the fixed switching frequency (f_{sw}) of 5 kHz for a fair comparison. For $f_s = 20$ kHz and $f_{sw} = 5$ kHz, the horizon length for the constrained mode is selected by $N = 20/5 = 4$. Note that the switching frequency (f_{sw}) is selected as 5 kHz by considering the tradeoff between the control performance and the efficiency with low switching loss. From $f_{sw} = 5$ kHz, the LC parameters are designed to filter out the f_{sw} and its harmonics. After designing the cutoff frequency that is suitable for this system, the capacitance C_f (6.6 μF) is first selected to reduce the no-load current in capacitor and its hardware cost based on the capacitors available commercially, and then the inductance L_f (10 mH) is properly chosen. Table I summarizes the main parameters of the experimental setup.

Remark 4: Due to the technological advancements of the recent DSP, the proposed MPC scheme can be readily implemented on the DSP platform as the observer-based LQR [7] and other advanced control algorithms ([8], [9], and [11]). To reduce the online computational burden, the unconstrained feedback gain matrix K in (19) as well as the constant matrices (Ψ and Φ) in (29) are calculated offline in advance. Most online computations of the proposed MPC method are in the exhaustive search in the constrained mode with seven options (i.e., equal to the options of the conventional FCS-MPC [20] as shown in Fig. 4 for $N = 6$). Because the allowable computation time for the compared control methods is within one sampling period and the conventional FCS-MPC [20] can work with a sampling frequency $f_s = 30$ kHz, the proposed algorithm can readily work with $f_s = 20$ kHz, as shown in the following experiments.

B. Dynamic Response Investigation via Flexible Performance Index

This section investigates the dynamic response of the proposed MPC method that depends on the performance index (16) accompanied by the practical rules to select the weight matrices Q and R. In (16), there is a tradeoff between control performance (V_{Le}^{++}) and control effort (V_{ie}) [7], [29], or in other words, between Q and R. Since two terms in (16) (V_{Le}^{++} and V_{ie}) have the same unit (voltage) and each term has two equivalent dimensions (i.e., $d-q$ components in the rotating reference frame), the weighting matrices $(P,\ R)$ can be simply selected as $P = I_{2\times 2}$ and $R = \varepsilon I_{2\times 2}$, where ε is a positive real number called the weighting factor. Then, the choice of the weighting matrices can be simplified with only one weighting factor ε. In the constrained mode, a fast dynamic response is desired, so the aggressive performance is achieved by selecting a small ε (i.e., a large Q and a small R). In the unconstrained mode, good performances (i.e., low THD, small SSE, noise rejection, etc.) in the steady state are required, so a proper tuning of the performance index is needed with a larger ε (i.e., a smaller Q and a larger R) compared with the constrained mode. Note that the proposed MPC allows the different selection of Q and R in two independent modes to avoid the tradeoff between Q and R in the LQR, so the proposed MPC method is much simpler than the LQR in [7] regarding the weight tuning procedure.

Fig. 6(a) shows the comparative dynamic performances of the conventional LQR and the proposed MPC when the reference output voltage (V_{Ld}^*) is step changed at no-load condition. Note that only V_{Ld}^* is step changed in this test, so the V_{Ld} waveform is included in Fig. 6(a) to show the voltage tracking performance. The waveforms of the conventional LQR with a large ε (i.e., $\varepsilon = 10$) locating at the upper position (i) show a long rising time of 25 ms (V_{Ld}) to track the reference $(V_{Ld}^* = 155.56\,\mathrm{V})$, but less ripples (V_{LA}) in the steady state with THDs $= 0.70\%$. Next, the waveforms of the conventional LQR with a small ε (i.e., $\varepsilon = 0.1$) in the middle position (ii) exhibit a short rising time of 2.0 ms (V_{Ld}), but more ripples (V_{LA}) in the steady state with THD $= 1.60\%$. Therefore, there is a tradeoff between the desired performances in the transient-state and the steady state in case of the conventional LQR. Finally, the waveforms of the proposed MPC in the lower position (iii) indicate both a short rising time of 1.8 ms (V_{Ld}) and less ripples (V_{LA}) in the steady state with THD $= 0.65\%$, which confirm the distinguished advantages of the proposed flexible-mode design.

To further investigate the efficacy of the proposed long-horizon MPC in the constrained mode, Fig. 6(b) illustrates the dynamic response of the proposed MPC with respect to different horizon lengths $N = 2,\ 4,\ 6$ in case of a step-changed reference (i.e., V_{Ld}^* changes from 0 to 155.6 V). As seen in Fig. 6(b), there are significant improvements of the dynamic response when N increases from 2 to 4. However, when N increases from 4 to 6, the dynamic performance is negligibly improved. It is noted that the remarkable improvements in the constrained mode are achieved due to the effectiveness of the long-horizon prediction over H1-MPC.

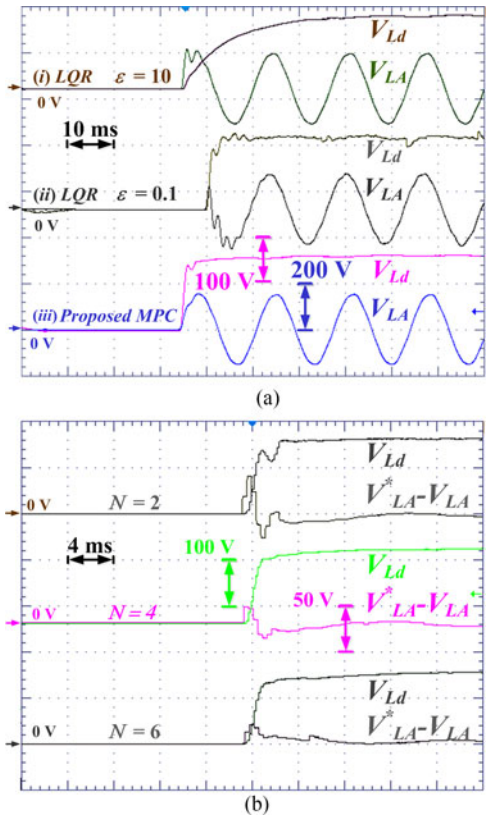

Fig. 6. Dynamic response investigation under a step-changed reference at no-load condition. (a) Comparative dynamic response with (i) the conventional LQR at a low gain ($\varepsilon = 10$), (ii) the conventional LQR at a high gain ($\varepsilon = 0.1$), and (iii) the proposed MPC at flexible modes. (b) Dynamic response of the proposed MPC method in the constrained mode via different prediction horizon lengths (i.e., $N = 2, 4, 6$).

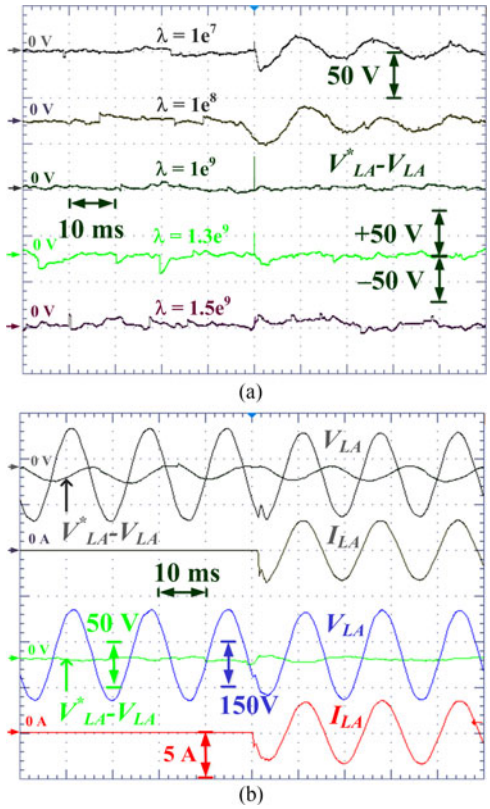

Fig. 7. Robust performances of the proposed disturbance-rejection-based MPC method under incorrectly set values of L and C. (a) Voltage errors (phase A) of the proposed MPC method under different DOB gains. (b) Comparative controlled outputs of the conventional LQR (upper position) and the proposed MPC (lower position).

C. Robustness Investigation via DOB Performance

This section evaluates the robustness of the proposed disturbance-rejection-based MPC method by investigating the insensitivity of the controlled output voltage against the parameter uncertainties under a load step-change condition.

To realize the parameter uncertainties, the values of L and C are set in the control algorithm program with significant distortions (i.e., $+100\%$ and -50% from the nominal values of both L and C provided by the manufacturers). Note that the parameter changes in the control program are also widely used in the literature [30] to evaluate the control robustness because this method can avoid the filtering deterioration due to the physical change of an LC filter. Fig. 7(a) shows the error dynamics of phase A voltage under parameter mismatches by incorrectly set parameters (i.e., -50% parameter uncertainties with half of the nominal values $L_f = 0.5 \times 10 = 5\,\text{mH}$, $C_f = 0.5 \times 6.6 = 3.3\,\mu\text{F}$) when the load is step changed. The waveforms shown in Fig. 7(a) reveal the effectiveness of the DOB on removing the SSE and improving the controlled output with different observer gain settings via λ where $Q_0 = \lambda R_0$. In this paper, the effective weighting matrices Q_0 and R_0 are selected via the weighting factor $\lambda = 1e^9$.

Next, Fig. 7(b) shows the comparative output waveforms of the conventional LQR and the proposed MPC in case of incorrectly set parameters (i.e., $+100\%$ parameter uncertainties with double of nominal values, $L_f = 2.0 \times 10 = 20\,\text{mH}$, $C_f = 2.0 \times 6.6 = 13.2\,\mu\text{F}$). As observed from Fig. 7(b), the conventional LQR (upper position) exhibits a very large SSE of 9.5 V (6.1%), whereas the proposed MPC shows a small SSE of 0.5 V (0.3%). In this figure, the THDs of the phase A voltage are 0.75% and 0.65%, respectively.

To this end, the disturbance-rejection approach contributes reasonably to the reduction of the SSE in case of high parameter uncertainties (100%). It is worth mentioning that this paper investigates the highly distorted values of both *L* and *C* in comparison with recently published results in the same topics [7], [18]–[20], whereas the most common tolerances of the *LC* values are provided by the manufacturers [7] within $\pm 10\%$ around the nominal values.

D. Comparative Studies Under a Linear Load Step Change

Fig. 8 shows the comparative performance of the conventional LQR and the proposed MPC under a linear load step change with subfigures (a) and (b), respectively. As depicted in Fig. 8(a), the conventional LQR shows the sinusoidal waveforms of $\bar{V}_L = [V_{LA}\ V_{LB}\ V_{LC}]^T$ in the steady state with the voltage error of 0.8 V and the THD of 0.75%. Under a sudden disturbance by the load step change, the recovering time of the conventional LQR

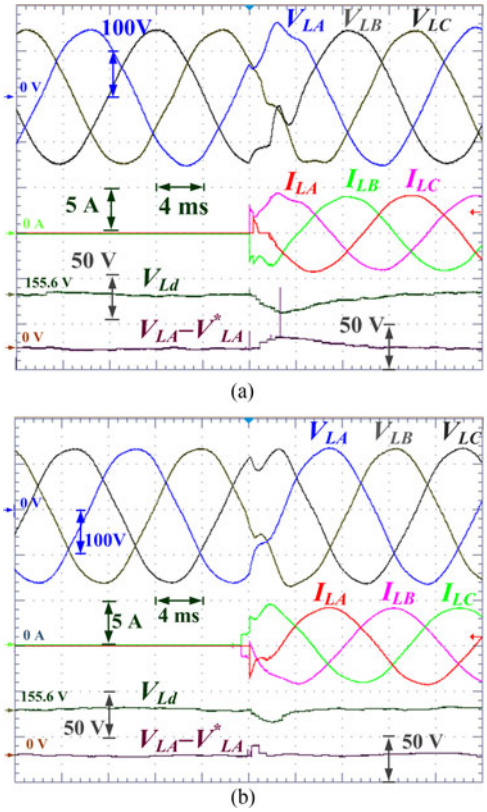

Fig. 8. Comparative performance under a linear load step change. (a) Conventional LQR. (b) Proposed MPC.

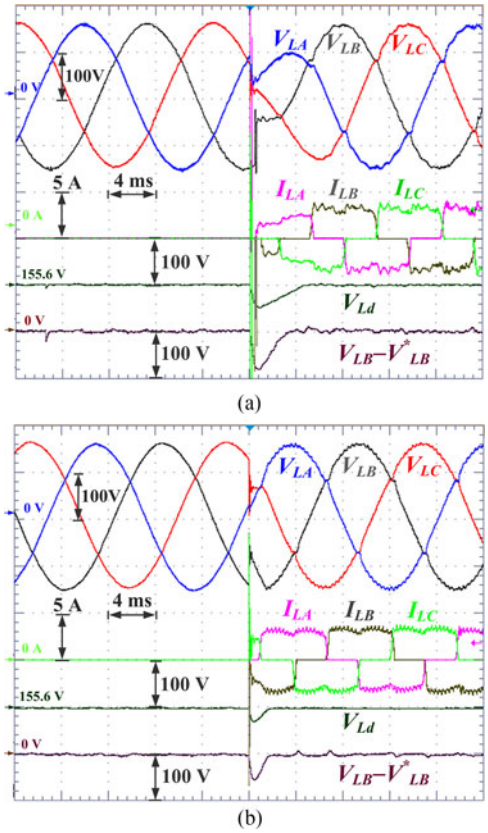

Fig. 9. Comparative performance under a nonlinear load step change. (a) Conventional LQR. (b) Proposed MPC.

is 6.5 ms with voltage spikes (52 V in phase A) and the voltage dip is 18.0 V. Meanwhile, Fig. 8(b) shows the performance of the proposed MPC with sinusoidal voltages in the steady state. In this figure, the measured SSE is 0.3 V and the THD is 0.7%. In the transient state by a load step change, the recovering time of the proposed MPC is 2.8 ms and the voltage dip is 18.0 V.

In the case of a load step change, both schemes show the competitive steady-state voltage regulation (e.g., the SSE and THD). However, the proposed MPC shows better results with much faster dynamic response with smooth voltage recovering (i.e., V_{Ld} and $V_{LA} - V^*_{LA}$) due to the proposed long-horizon MPC. Furthermore, the steady-state performance of the proposed MPC shows a smaller SSE with nearly zero SSE and a smaller THD due to the proposed disturbance-rejection approach. Specially, there is no overshoot in the transient state of the proposed MPC, whereas the voltage waveforms of the conventional LQR in Fig. 8(a) show some overshoot and spikes. This confirms the important advantages of the proposed MPC on the constraints handling along with the optimality.

E. Comparative Studies Under a Nonlinear Load Step Change

Fig. 9 shows the comparative performance of the two control schemes (i.e., the conventional LQR and the proposed MPC) under a nonlinear load step change with a three-phase diode rectifier circuit (i.e., $L_r = 5\,\text{mH}$, $C_r = 50\,\mu\text{F}$, and $R_r = 60\,\Omega$). Fig. 9(a) and (b) shows the following waveforms of the conventional LQR and the proposed MPC: three-phase controlled outputs $\bar{\boldsymbol{V}}_L = [V_{LA}\, V_{LB}\, V_{LC}]^T$, load phase currents $\bar{\boldsymbol{I}}_L = [I_{LA}\, I_{LB}\, I_{LC}]^T$, d-axis load voltage V_{Ld}, and the phase B voltage error $V_{LB} - V^*_{LB}$.

First, Fig. 9(a) shows the experimental results of the conventional LQR under a nonlinear load step change. In this figure, it is observed that in the transient state under the step change, the recovering time of the conventional LQR is 4.8 ms and its dip voltage is 92 V. In the steady state under a nonlinear load, the controlled output voltages contain some distortion due to the high-harmonic components of the nonlinear load currents. In this case, the THD and SSE are 2.6% and 1.5 V, respectively. Next, Fig. 9(b) shows the control performance of the proposed MPC with the comparative waveforms shown in Fig. 9(a). In the transient-state under the step change, the proposed MPC exhibits a good dynamic response with a small recovering time (about 1.8 ms) and a reduced voltage dip (48 V). In the steady state under the same nonlinear load, the THD and SSE are 1.4% and 0.25 V, respectively.

Thus, both control methods show acceptable controlled outputs regarding the THDs and SSEs in the steady state of a nonlinear load condition. Nevertheless, the proposed MPC method shows better control performances (i.e., lower THDs, smaller SSEs, shorter recovering time, and less voltage dip) in both the steady state and the transient state in comparison with the conventional LQR. These experimental results once again confirm the advantages of the flexible-mode design based on MPC. That

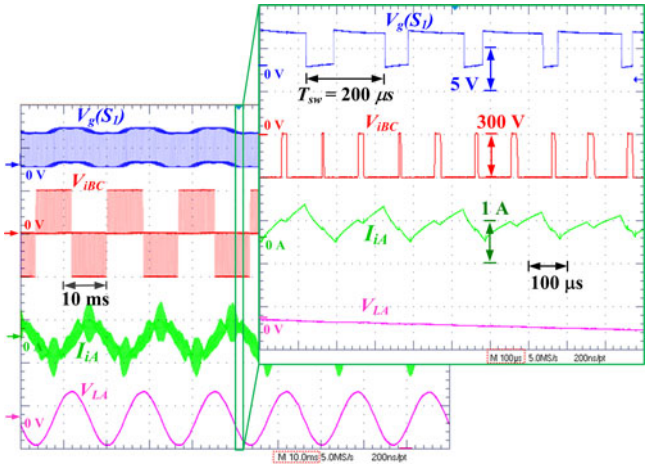

Fig. 10. PWM driving signal $(V_g(S_1))$ from DSP for the switch S_1, inverter line-to-line voltage (V_{iBC}), and inverter line current (I_{iA}) of the proposed MPC in the no-load condition to show the switching frequency.

TABLE II
COMPARATIVE PERFORMANCES BETWEEN THE CONVENTIONAL LQR AND THE PROPOSED MPC

	Steady-States			No Load	Full Load	Nonlinear Load
The conventional LQR①/ The Proposed MPC②	THD (%)		①/②	0.7/0.65	0.75/0.7	2.6/1.4
	Steady-State Error (V_{rms})	V_{LA}		1.1/0.3	0.8/0.3	1.5/0.25
		V_{LB}		1.0/0.35	0.7/0.25	1.4/0.2
		V_{LC}		1.0/0.3	0.8/0.3	1.5/0.25
	Transient-States			Linear-Load Step-Change		Nonlinear Load Step-Change
	Recovering Time (ms)		①/②	6.5/2.8		4.8/1.8
	Dip Voltage (V)			18/18		92/48

is, the superior steady-state performances are achieved from the simple H1-MPC and DOB. On the other hand, the long-horizon MPC can further optimize the modulation stage to achieve fast dynamics in the transient state.

Fig. 10 shows the PWM driving signal $(V_g(S_1))$ from DSP for the switch S_1, the inverter line-to-line voltage (V_{iBC}), and the inverter line current (I_{iA}) of the proposed MPC in the no-load condition in order to exhibit the fixed switching frequency $(f_{sw} = 5\,\text{kHz})$. In this figure, the phase A load voltage (V_{LA}) is also presented to show the regulating performance of the proposed MPC for the three-phase inverter with an LC filter. Note that the benefits of a fixed switching frequency scheme over a variable switching frequency one can be listed as: the EMI filter design is easier, the switching loss is even distributed over the switches to avoid local overheating, and the unwanted resonances due to the self-resonance frequency of the LC filter are also eliminated [21], [23]. Finally, Table II summarizes the comparative performances between the conventional LQR and the proposed MPC in both the steady state and transient state.

VI. CONCLUSION

This paper proposed a flexible-mode MPC based on the disturbance-rejection approach for three-phase VSIs. The proposed MPC approach utilizes the H-1 MPC law in the unconstrained mode and the long-horizon MPC law in the constrained mode. By using two flexible modes, the proposed MPC technique can achieve the performance improvements in both transient state and steady state that are validated by comparative experimental results. In this paper, the H1-MPC control law was appropriately derived by relating the H1-MPC to the deadbeat controller and the LQR with guaranteed closed-loop stability. Also, the long-horizon MPC was efficiently solved by using the finite switching sequences of the sector-based modulation. Consequently, the proposed disturbance-rejection-based MPC approach offers more robustness and more precise voltage regulation under high uncertainties of L and C values in comparison with the conventional LQR.

REFERENCES

[1] F. Blaabjerg, R. Teodorescu, M. Liserre, and A. V. Timbus, "Overview of control and grid synchronization for distributed power generation systems," *IEEE Trans. Ind. Electron.*, vol. 53, no. 5, pp. 1398–1409, Oct. 2006.
[2] J. M. Carrasco *et al.*, "Power-electronic systems for the grid integration of renewable energy sources: A survey," *IEEE Trans. Ind. Electron.*, vol. 53, no. 4, pp. 1002–1016, Aug. 2006.
[3] M. Shahparasti, M. Mohamadian, A. Yazdian, A. A. Ahmad, and M. Amini, "Derivation of a stationary-frame single-loop controller for three-phase standalone inverter supplying nonlinear loads," *IEEE Trans. Power Electron.*, vol. 29, no. 9, pp. 5063–5071, Sep. 2014.
[4] P. C. Loh, M. J. Newman, D. N. Zmood, and D. G. Holmes, "A comparative analysis of multiloop voltage regulation strategies for single and three-phase UPS systems," *IEEE Trans. Power Electron.*, vol. 18, no. 5, pp. 1176–1185, Sep. 2003.
[5] F. Bosio, L. A. D. Ribeiro, F. D. Freijedo, M. Pastorelli, and J. M. Guerrero, "Effect of state feedback coupling and system delays on the transient performance of stand-alone VSI with LC output filter," *IEEE Trans. Ind. Electron.*, vol. 63, no. 8, pp. 4909–4918, Aug. 2016.
[6] P. C. Loh and D. G. Holmes, "Analysis of multiloop control strategies for *LC*/*CL*/*LCL*-filtered voltage-source and current-source inverters," *IEEE Trans. Ind. Appl.*, vol. 41, no. 2, pp. 644–654, Mar./Apr. 2005.
[7] E. K. Kim, F. Mwasilu, H. H. Choi, and J. W. Jung, "An observer-based optimal voltage control scheme for three-phase UPS systems," *IEEE Trans. Ind. Electron.*, vol. 62, no. 4, pp. 2073–2081, Apr. 2015.
[8] T. D. Do, V. Q. Leu, Y. S. Choi, H. H. Choi, and J. W. Jung, "An adaptive voltage control strategy of three-phase inverter for stand-alone distributed generation systems," *IEEE Trans. Ind. Electron.*, vol. 60, no. 12, pp. 5660–5672, Dec. 2013.
[9] T. D. Nguyen, H. H. Lee, and H. M. Nguyen, "Adaptive carrier-based PWM for a four-switch three-phase inverter under DC-link voltage ripple conditions," *J. Elect. Eng. Technol.*, vol. 5, no. 2, pp. 290–298, Jun. 2010.
[10] G. Escobar, A. A. Valdez, J. Leyva-Ramos, and P. Mattavelli, "Repetitive-based controller for a UPS inverter to compensate unbalance and harmonic distortion," *IEEE Trans. Ind. Electron.*, vol. 54, no. 1, pp. 504–510, Feb. 2007.
[11] W. Z. Lu, K. L. Zhou, D. W. Wang, and M. Cheng, "A general parallel structure repetitive control scheme for multiphase DC–AC PWM converters," *IEEE Trans. Power Electron.*, vol. 28, no. 8, pp. 3980–3987, Aug. 2013.
[12] S. Jiang, D. Cao, Y. Li, J. F. Liu, and F. Z. Peng, "Low-THD, fast-transient, and cost-effective synchronous-frame repetitive controller for three-phase UPS inverters," *IEEE Trans. Power Electron.*, vol. 27, no. 6, pp. 2994–3005, Jun. 2012.
[13] F. Hamoudi, A. A. Chaghi, H. Amimeur, and A. K. Merabet, "Sliding mode control with fixed switching frequency for four-wire shunt active filter," *J. Elect. Eng. Technol.*, vol. 6, no. 5, pp. 647–657, Sep. 2011.
[14] H. Komurcugil, "Rotating-sliding-line-based sliding-mode control for single-phase UPS inverters," *IEEE Trans. Ind. Electron.*, vol. 59, no. 10, pp. 3719–3726, Oct. 2012.
[15] T. Kawabata, T. Miyashita, and Y. Yamamoto, "Dead beat control of three phase PWM inverter," *IEEE Trans. Power Electron.*, vol. 5, no. 1, pp. 21–28, Jan. 1990.
[16] P. Mattavelli, "An improved deadbeat control for UPS using disturbance observers," *IEEE Trans. Ind. Electron.*, vol. 52, no. 1, pp. 206–212, Feb. 2005.

[17] J. S. Lim, C. Park, J. Han, and Y. I. Lee, "Robust tracking control of a three-phase DC-AC inverter for UPS applications," *IEEE Trans. Ind. Electron*, vol. 61, no. 8, pp. 4142–4151, Aug. 2014.
[18] S. K. Kim, C. R. Park, T. W. Yoon, and Y. I. Lee, "Disturbance-observer-based model predictive control for output voltage regulation of three-phase inverter for uninterruptible-power-supply applications," *Eur. J. Control*, vol. 23, pp. 71–83, May 2015.
[19] J. F. Hu, J. G. Zhu, and D. G. Dorrell, "Model predictive control of inverters for both islanded and grid-connected operations in renewable power generations," *IET Renewable Power Gen.*, vol. 8, no. 3, pp. 240–248, Apr. 2014.
[20] P. Cortes, G. Ortiz, J. I. Yuz, J. Rodriguez, S. Vazquez, and L. G. Franquelo, "Model predictive control of an inverter with output LC filter for UPS applications," *IEEE Trans. Ind. Electron.*, vol. 56, no. 6, pp. 1875–1883, Jun. 2009.
[21] S. Vazquez *et al.*, "Model predictive control a review of its applications in power electronics," *IEEE Ind. Electron. Mag.*, vol. 8, no. 1, pp. 16–31, Mar. 2014.
[22] H. A. Young, M. A. Perez, J. Rodriguez, and H. Abu-Rub, "Assessing finite-control-set model predictive control a comparison with a linear current controller in two-level voltage source inverters," *IEEE Ind. Electron. Mag.*, vol. 8, no. 1, pp. 44–52, Mar. 2014.
[23] J. Rodriguez *et al.*, "State of the art of finite control set model predictive control in power electronics," *IEEE Trans. Ind. Informat.*, vol. 9, no. 2, pp. 1003–1016, May 2013.
[24] R. P. Aguilera and D. E. Quevedo, "Predictive control of power converters: Designs with guaranteed performance," *IEEE Trans. Ind. Informat.*, vol. 11, no. 1, pp. 53–63, Feb. 2015.
[25] R. P. Aguilera, P. Lezana, and D. E. Quevedo, "Switched model predictive control for improved transient and steady-state performance," *IEEE Trans. Ind. Informat.*, vol. 11, no. 4, pp. 968–977, Aug. 2015.
[26] D. E. Quevedo, R. P. Aguilera, and T. Geyer, "Predictive control in power electronics and drives: Basic concepts, theory, and methods," in *Advanced and Intelligent Control in Power Electronics and Drives*, vol. 531, no. 5. New York, NY, USA: Springer, 2014, pp. 181–226.
[27] S. Vazquez, J. Rodriguez, M. Rivera, L. G. Franquelo, and M. Norambuena, "Model predictive control for power converters and drives: Advances and trends," *IEEE Trans. Ind. Electron.*, vol. 64, no. 2, pp. 935–947, Feb. 2017.
[28] K. Ogata, *Discrete-Time Control Systems*, 2nd ed. Englewood Cliffs, NJ, USA: Prentice-Hall, 1994.
[29] E. Mosca, *Optimal, Predictive, and Adaptive Control*, Englewood Cliffs, NJ, USA: Prentice-Hall, 1995.
[30] M. Ghanes, M. Trabelsi, H. Abu-Rub, and L. Ben-Brahim, "Robust adaptive observer based model predictive control for multilevel flying capacitors inverter," *IEEE Trans. Ind. Electron.*, vol. 63, no. 12, pp. 7876–7886, Dec. 2016.

Hoach The Nguyen received the B.S. degree from Hanoi University of Science and Technology, Hanoi, Vietnam, and the M.S. degree from Dayeh University, Changhua, Taiwan, in 2007 and 2010, respectively, both in electrical engineering.

He is currently working toward the Ph.D. degree in the Division of Electronics and Electrical Engineering, Dongguk University, Seoul, South Korea. From 2011 to 2014, he was a Lecturer at Hanoi Architecture University, Hanoi, Vietnam. His research interests include electric power system, control of power converters, and DSP-based electric machine drives.

Jin-Woo Jung (M'06) received the B.S. and M.S. degrees in electrical engineering from Hanyang University, Seoul, South Korea, and the Ph.D. degree in electrical and computer engineering from The Ohio State University, Columbus, OH, USA, in 1991, 1997, and 2005, respectively.

From 1997 to 2000, he was in the Home Appliance Research Laboratory, LG Electronics Co., Ltd., Seoul, South Korea. From 2005 to 2008, he was a Senior Engineer in the R&D Center and in the PDP Development Team, Samsung SDI Co., Ltd., Seoul, South Korea. Since 2008, he has been a Professor in the Division of Electronics and Electrical Engineering, Dongguk University, Seoul, South Korea. His research interests include DSP-based electric machine drives, distributed generation systems using renewable energy sources, and power conversion systems and drives for electric vehicles.